LETTER

doi:10.1038/nature12236

Behaviour-dependent recruitment of long-range projection neurons in somatosensory cortex

Jerry L. Chen[1], Stefano Carta[1,2], Joana Soldado-Magraner[1,3], Bernard L. Schneider[4] & Fritjof Helmchen[1,2]

In the mammalian neocortex, segregated processing streams are thought to be important for forming sensory representations of the environment[1,2], but how local information in primary sensory cortex is transmitted to other distant cortical areas during behaviour is unclear. Here we show task-dependent activation of distinct, largely non-overlapping long-range projection neurons in the whisker region of primary somatosensory cortex (S1) in awake, behaving mice. Using two-photon calcium imaging, we monitored neuronal activity in anatomically identified S1 neurons projecting to secondary somatosensory (S2) or primary motor (M1) cortex in mice using their whiskers to perform a texture-discrimination task or a task that required them to detect the presence of an object at a certain location. Whisking-related cells were found among S2-projecting (S2P) but not M1-projecting (M1P) neurons. A higher fraction of S2P than M1P neurons showed touch-related responses during texture discrimination, whereas a higher fraction of M1P than S2P neurons showed touch-related responses during the detection task. In both tasks, S2P and M1P neurons could discriminate similarly between trials producing different behavioural decisions. However, in trials producing the same decision, S2P neurons performed better at discriminating texture, whereas M1P neurons were better at discriminating location. Sensory stimulus features alone were not sufficient to elicit these differences, suggesting that selective transmission of S1 information to S2 and M1 is driven by behaviour.

In the whisker region of S1 (also known as the barrel cortex), layer 2/3 (L2/3) pyramidal neurons send direct projections to S2 and M1 in a generally non-overlapping manner[3–6]. We used a combination of viral-based and synthetic retrograde tracers to label uniquely these long-range projection neurons (Fig. 1a and Supplementary Fig. 1). Using adult transgenic Cre-dependent tdTomato reporter mice[7], we injected a retrograde-infecting adeno-associated virus (AAV, serotype 6) expressing Cre recombinase (AAV6-*Cre*)[3] into S2 to induce long-term tdTomato expression in S2P neurons, later visualized *in vivo* (Fig. 1b and Supplementary Fig. 2a). M1P neurons were labelled by M1 injection of cholera toxin subunit B (CTB, also known as CtxB) conjugated to Alexa647 (CTB-Alexa647) and retrospectively identified in fixed tissue sections. These tracers exhibit similar relative efficiency, labelling a maximum of approximately 80% of all projection neurons to the injection site (Supplementary Fig. 2b–f). For calcium imaging, we injected into S1 an AAV6 expressing yellow-cameleon Nano140 (YC-Nano140)[8], a sensitive genetically encoded calcium indicator that reliably reports action-potential firing (Supplementary Fig. 3). Similar to previous reports[5,6], we found that S2P and M1P neurons constitute a spatially intermingled, largely non-overlapping population with only a small fraction (approximately 10%) of co-labelled neurons (neurons expressing both S2P and M1P, which we refer to here as 'S2P/M1P' neurons). In addition, post-hoc GABA (γ-aminobutyric acid) immunohistochemistry confirmed that labelled S2P and M1P neurons are non-GABAergic (Supplementary Fig. 4).

Mice use their whiskers to discriminate fine tactile features and to determine an object's position[1]. We first measured neuronal firing of long-range projection neurons in mice trained to perform an S1-dependent texture discrimination task[9–12] under head-fixed conditions, enabling simultaneous two-photon imaging (Fig. 1c, d). Using a 'go/no-go' behaviour paradigm, mice were trained for 'go' trials to lick for a water reward ('hit') when presented with a target texture, a panel of coarse sandpaper (P100); and for 'no-go' trials to withhold licking ('correct rejection') when presented with one of three non-rewarded, 'non-target' textures of increasingly smoother grades (P280, P600, P1200) (Supplementary Fig. 5 and Supplementary Videos 1 and 2). Misses on go trials were not rewarded, and false alarms on no-go trials were punished with an air puff and a time-out period.

Calcium imaging of S1 projection neurons was carried out in six expert mice while whisker motion and texture contact were monitored using high-speed videography (Fig. 1e and Supplementary Video 3). We measured neuronal activity across tens of labelled cells, sampling different neurons across imaging sessions. We analysed 679 neurons, including 161 S2P, 118 M1P, 31 S2P/M1P, and 369 unlabelled neurons (for S2P/M1P neuron analysis, see Supplementary Table 1). Unlabelled neurons probably consist of a mixed population of unlabelled S2P or M1P neurons, and neurons not projecting to these areas. Responses in S1 were sparse, with 34% of L2/3 neurons showing activity during the behaviour session. S1 neurons are responsive to both whisker motion during free whisking[13,14] and sensory input from whisker touch[15–17]. Our image acquisition rate was too low to observe locking of neuronal responses with rhythmic whisking[15] or surface palpitations[9], so for a simple functional classification we cross-correlated cellular calcium signals across all trials against the envelope of whisking amplitude and a binary vector representing touch periods, respectively (Fig. 1f, g). Based on positive correlation peaks within defined lag time windows and significant differences in the two correlations, cells were classified as 'whisking' or 'touch' cells; cells remained 'unclassified' when no significant positive correlation to whisking or touch existed or correlation peaks occurred outside of the lag windows (see Methods and Supplementary Fig. 6). A large fraction of active S2P neurons (47%) were responsive to touch, higher compared to M1P and unlabelled neurons ($P < 0.05$, bootstrap test; Fig. 1h). Notably, whisking cells were identified among S2P and unlabelled neurons but not among M1P neurons, suggesting that whisking information arriving in S1 from the sensory periphery[14] or from M1 (refs 18, 19) is transmitted to S2 but not to M1 (ref. 20). Estimates of neuronal firing from calcium signals (Supplementary Fig. 3e) indicate that unclassified neurons were less active than touch or whisking neurons (Supplementary Fig. 7a–c). It is unclear whether unclassified neurons are relevant to task behaviour or simply exhibit spontaneous activity.

We next examined how S2P or M1P neurons might contribute to sensory coding or decision making during texture discrimination. Individual neurons exhibited diverse responses and selectivity to trial type and texture (Fig. 2a, b). To quantify how well single cells could

[1]Brain Research Institute, University of Zurich, Winterthurerstrasse 190, CH-8057 Zurich, Switzerland. [2]Neuroscience Center Zurich, University of Zurich/ETH Zurich, Winterthurerstrasse 190, CH-8057 Zurich, Switzerland. [3]Institute of Neuroinformatics, University of Zurich/ETH Zurich, Winterthurerstrasse 190, CH-8057 Zurich, Switzerland. [4]Brain Mind Institute, Ecole Polytechnique Fédérale de Lausanne (EPFL), EPFL SV BMI LEN, Station 19, CH-1015 Lausanne, Switzerland.

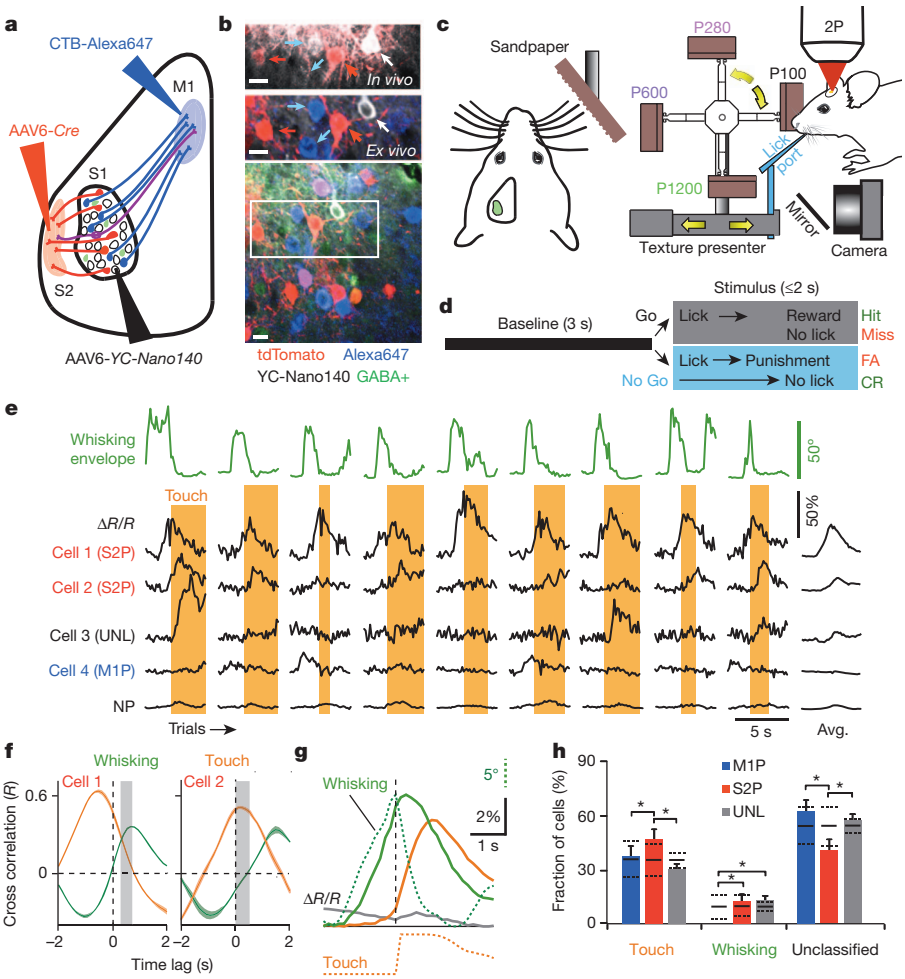

Figure 1 | *In vivo* calcium imaging of long-range projection neurons in S1 during texture discrimination. **a**, Retrograde labelling of S2P and M1P neurons in S1 by AAV6-*Cre* and CTB-Alexa647 injection, respectively. AAV6-*YC-Nano140* was injected into S1 for calcium imaging. **b**, Top, *in vivo* image of L2/3 neurons in S1 expressing YC-Nano140 (white). AAV6-*Cre*-infected S2P neurons express tdTomato (red). Middle and bottom (lower magnification), post-hoc identification of *in vivo* imaged neurons with CTB-Alexa647-labelled M1P neurons (blue) and immunostained GABA-positive neurons (green). Scale bar, 20 μm. **c**, Setup for two-photon (2P) imaging of S1 neurons during head-fixed texture discrimination. **d**, Trial structure for go/no-go texture discrimination task. CR, correct rejection; FA, false alarm. **e**, Calcium transients (black) from example cells and the neuropil (NP) across nine trials, and the average trace across all trials. Envelope of whisking amplitude (green) and periods of touch (orange area) are also shown. UNL, unlabelled. **f**, Cross-correlation analysis of calcium signals with whisking amplitude (green) and touch (orange) across different time lags for 'whisking' (cell 1) and 'touch' (cell 2) in **e**. Shaded trace indicates 95% confidence interval from bootstrap test. Grey area indicates lag window for classification. **g**, Average calcium trace across all whisking (green), touch (orange), and unclassified (grey) neurons shown with average whisking amplitude and touch vectors (dotted lines). **h**, Distribution of classified cells across subtypes. Error bars, s.d. from bootstrap test. A permutation test of shuffled labels are shown. Solid horizontal lines, means; dashed horizontal lines, 95% confidence intervals ($n = 231$ active neurons). $^*P < 0.05$.

discriminate between any given two conditions, between the reported decision of hit versus correct rejection or between two distinct textures, we performed a receiver operating characteristic (ROC) analysis[16,21] (Fig. 2c; see Supplementary Fig. 8 for neuronal populations). When comparing hit and correct rejection trials, we found that 49% of S2P neurons discriminated these trial types above chance, a higher percentage than for M1P or unlabelled neurons ($P < 0.05$, bootstrap test; Fig. 2d). For analysis of texture coding, we focused only on pairs of non-target textures (non-rewarded stimuli, to which animals should respond by withholding licking) in correct rejection trials to control for behavioural responses. For each non-target texture pair, a larger fraction of active M1P neurons showed above-chance discriminative power compared to S2P neurons ($P < 0.05$, bootstrap test; Fig. 2d). However, although fewer in numbers, individual discriminative S2P neurons were more accurate than M1P neurons in discriminating P280 versus P600, and P280 versus P1200 textures ($P < 0.05$, one-way analysis of variance (ANOVA), Tukey's post-hoc test; Fig. 2e). Although discriminating cells were found in each behavioural category, touch-related neurons performed better than whisking or unclassified cells. We conclude that differences exist between M1P and S2P neurons with respect to the information available for texture coding and decision making.

We next asked whether these differences are intrinsic to these cell types or whether they are influenced by the sensory-processing requirements specific to this texture-discrimination task. We reasoned that a contrasting task with different requirements could result in a different set of activation patterns between M1P and S2P neurons. To address this, we trained a second set of mice ($n = 4$) to a variation of a head-fixed, go/no-go object-localization task (also known as 'object detection with distractors'[22]) previously reported to activate cortical circuits between S1 and M1 (refs 16, 18, 19, 23, 24) (Fig. 3a, b). In this task, mice are trained to use multiple whiskers to locate the same vertical pole presented at different positions along the anterior–posterior axis. The pole was presented at a fixed target location for go trials and at two non-target locations (+4.29 and +6 mm) anterior to the target location for no-go trials. We used an identical trial structure to the texture-discrimination task to control for non-sensory differences across tasks. Mice could reach similar performance levels[22] compared to texture

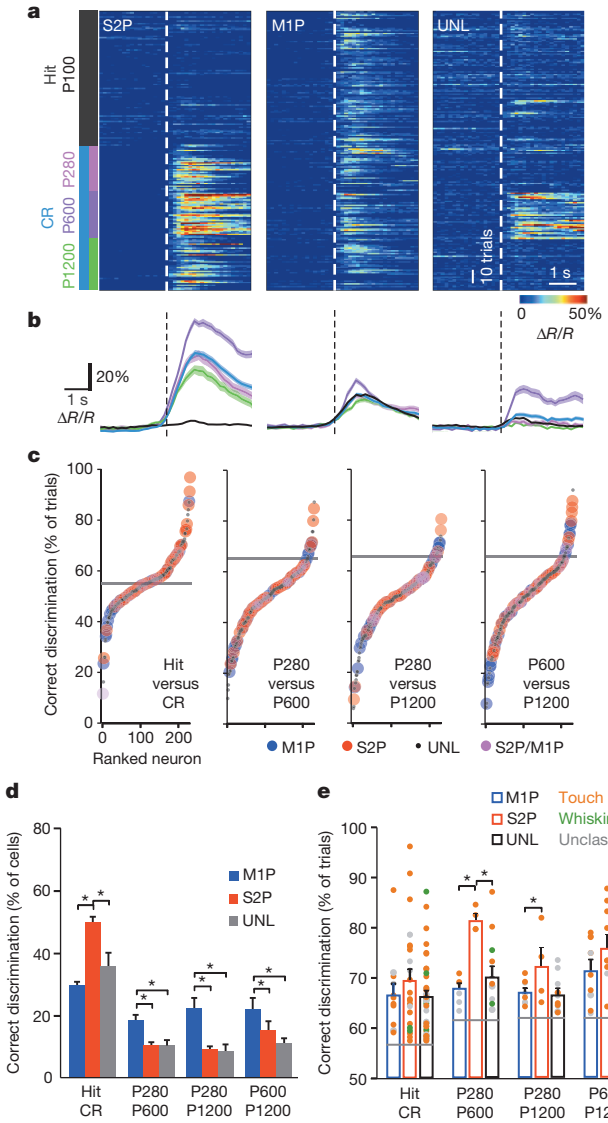

Figure 2 | Single-neuron discrimination analysis of decision or texture in S1 projection neurons. **a**, Single-trial responses of example S2P, M1P or UNL touch neurons to trial type or texture aligned to first touch (dotted line). **b**, Average calcium transient of neurons in **a** according to trial type or texture. Shaded areas, s.e.m. **c**, Fraction of trials in which individual cells correctly discriminated between decision (hit versus correct rejection) or between non-target textures from ROC analysis. Grey line indicates the 95th percentile of distribution from a permutation test of decision or texture labels. Neurons are ranked according to the fraction of trials that were correctly discriminated. Neurons above this line can discriminate above chance. **d**, Fraction of active cells discriminating trial type or texture above chance. **e**, Performance of neurons discriminating above chance. Circles indicate individual neurons shaded according to their behaviour classification. Grey lines indicate 95th percentile of distribution from a permutation test of decision or texture labels. Error bars, s.d. from a permutation test (**d**), s.e.m. (**e**). $n = 231$ active neurons; $^*P < 0.05$.

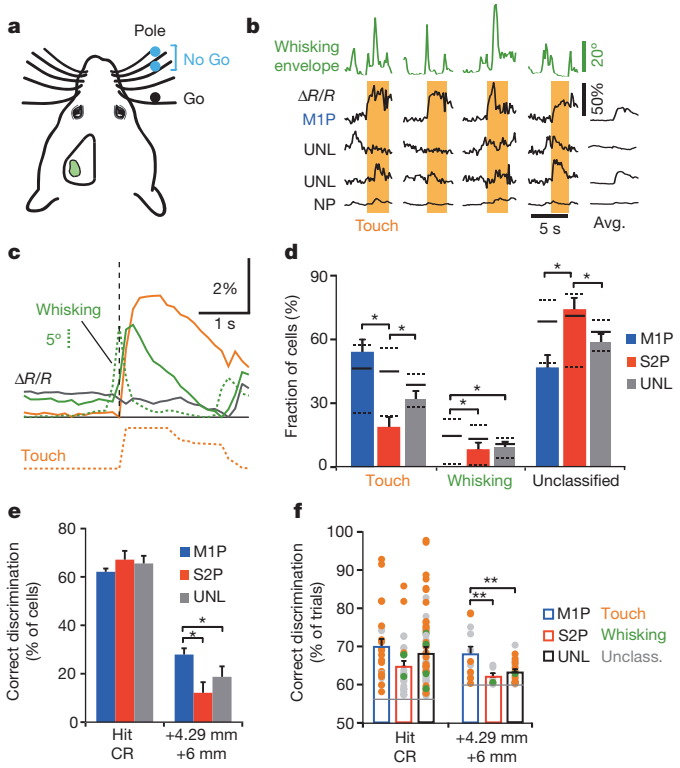

Figure 3 | Activity of S1 projection neurons during object localization. **a**, Positions of poles during the object-localization task. **b**, Calcium transients (black) of example cells and the neuropil (NP) across four trials, along with the average traces across all trials. Whisking amplitude (green) and periods of pole touch (orange area) are also shown. **c**, Average calcium trace across all whisking (green), touch (orange) and unclassified (grey) neurons shown with average whisking amplitude and touch vector (dotted lines). **d**, Distribution of classified cells across subtypes. A permutation test of shuffled labels is shown. Solid line, mean; dashed line, 95% confidence interval. **e**, Fraction of cells that discriminate decision or pole position above chance, from a ROC analysis. **f**, Performance of neurons discriminating above chance. Circles indicate individual neurons shaded according to behaviour classification. Grey line indicates the 95th percentile of distribution from a permutation test of decision or position labels. Error bars, s.d. from bootstrap test (**d**), s.d. from permutation test (**e**), s.e.m. (**f**). $n = 180$ active neurons; $^*P < 0.05$, $^{**}P < 0.01$.

discrimination (Supplementary Fig. 9). Calcium imaging in 386 neurons (84 M1P, 85 S2P, 19 S2P/M1P, and 198 unlabelled neurons) revealed a higher fraction of active cells (47%) compared to during texture discrimination. A large fraction of active M1P neurons (54%) were responsive to touch with a reduced representation (18%) in S2P neurons ($P < 0.05$, bootstrap test; Fig. 3c, d and Supplementary Fig. 7d–f). Similar to texture discrimination, no whisking-related M1P neurons were identified during object localization, demonstrating that this differential motor representation across projection neurons is intrinsic to the circuit. A ROC analysis revealed that similar fractions of S2P and M1P neurons could discriminate hit and correct rejection trials with similar performance levels (Fig. 3e, f and Supplementary Fig. 10). However, a larger fraction of M1P neurons could discriminate pole position at +4.29 mm from +6 mm compared to both S2P and unlabelled neurons ($P < 0.05$, bootstrap test) and with better accuracy ($P < 0.01$, one-way ANOVA, Tukey's post-hoc test; for touch neurons only see Supplementary Fig. 11).

The results suggest that, depending on task conditions, M1P and S2P neurons may be recruited in a manner necessary to perform sensory-driven, goal-directed behaviour. However, cell-type differences could arise simply from differences in physical stimuli used in each task. Indeed, fine-scale analysis of principal whisker kinematics showed that sandpaper and pole contacts showed distinct kinematic features. Changes in whisker curvature that relate to contact forces[22] as well as the frequency of high acceleration-velocity 'slip' events associated with texture coding[11,12] were greater during texture discrimination compared to object localization ($P < 0.001$, Kolmogorov–Smirnov test; Fig. 4a and Supplementary Fig. 12a). During object localization, pole contact by the principal whisker occurred along a greater range of angles ($P < 0.001$, F-test). In addition, contact occurred occasionally with different sets of whiskers across pole positions (Supplementary Fig. 13a, b). This pattern of whisker contact suggests that haptic sensing and labelled-line encoding strategies[24] are both available to the animal

in this task. We next asked whether S2P and M1P neurons show differential sensitivity to these parameters across tasks. Cross correlation with calcium signals of touch cells on correct rejection trials revealed diverse and sometimes high correlation with kinematic features (Fig. 4b, see also Supplementary Figs 12b and 13c, d). However, correlation of activity in S2P and M1P neurons to curvature change or mean touch angle were not different during both tasks. Although M1P neurons displayed higher correlation to slip events than S2P neurons, this difference was present during both task conditions (sandpaper, $P < 0.05$; pole, $P < 0.02$, one-way ANOVA, Tukey's post-hoc test; Fig. 4b). Thus, although differences exist in whisker kinematics, the cellular responses related to these parameters do not differ across cell types in a task-dependent manner.

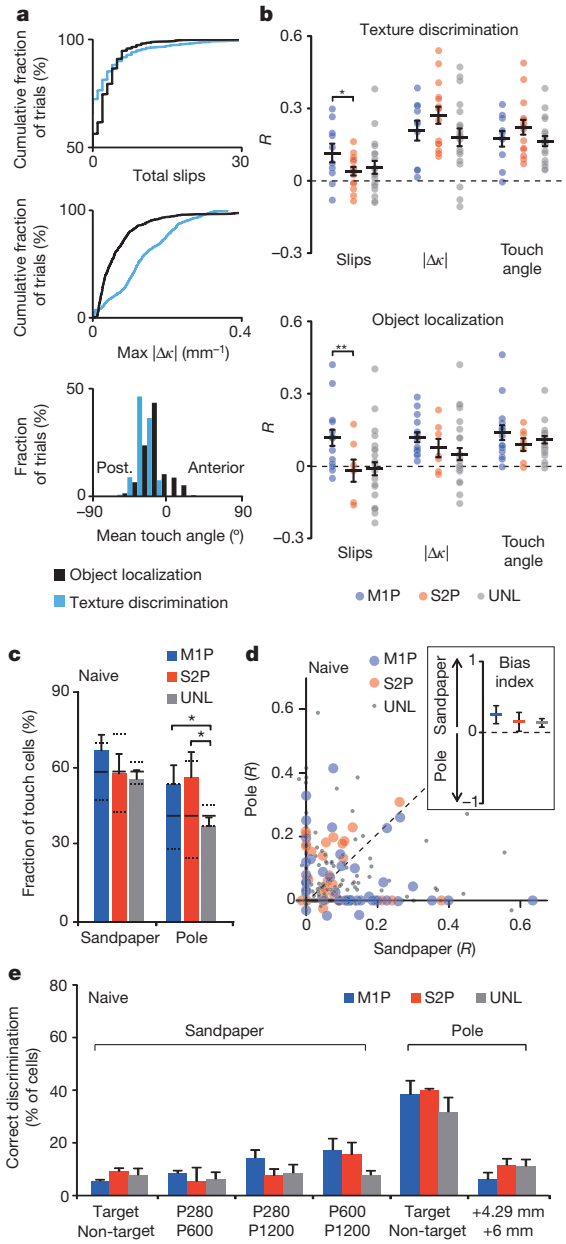

Figure 4 | Sensory stimuli are not sufficient to produce task-related differences. **a**, Whisker kinematic differences during texture discrimination versus object localization for high-acceleration-velocity 'slip' events, maximum absolute curvature change (max $|\Delta\kappa|$), mean touch angle (0° = orthogonal to anterior–posterior axis) over first second of touch. **b**, Cross correlation of calcium signals with whisker kinematic features for touch during texture discrimination (top panel) or object localization (bottom panel). **c**, Fraction of touch neurons identified by cross-correlation analysis from active neurons in naive animals. A permutation test of shuffled labels is shown. **d**, Cross correlation of calcium activity to sandpaper versus pole touch in naive animals. Inset, population bias index (see Methods) determined from the *R* value. **e**, Fraction of cells discriminating above chance for target versus non-target stimuli or between non-target stimuli, from a ROC analysis in naive animals. Error bars, s.e.m. (**a**), s.d. from a bootstrap test (**c**), s.d. from a permutation test (**c**). $n = 1{,}574$ trials (**a**), $n = 98$ touch neurons (**b**); $n = 207$ active neurons (**c**–**e**); $^{*}P < 0.05$, $^{**}P < 0.02$.

Given our limitations in temporal resolution to account for all aspects of touch-related neuronal activity during the complex, multi-whisker interactions, we also measured the responses of S2P and M1P neurons in naive, non-rewarded animals presented passively with both sandpaper and pole under simulated task conditions ($n = 5$ mice; 76 M1P, 58 S2P, 2 S2P/M1P, and 352 unlabelled neurons; summarized in Supplementary Fig. 7f). Similar fractions of active S2P and M1P neurons were responsive to touch for sandpaper and pole presentation (Fig. 4c). We found a diverse set of responses with certain neurons responding to either one or both stimuli but no difference in bias between S2P and M1P neurons (Fig. 4d). A ROC analysis showed a substantial reduction in the fraction of cells discriminating target versus non-target stimuli in naive animals, when compared to hit versus correct rejection trials in trained animals during texture discrimination and, to a lesser degree, during object localization ($P < 0.05$, bootstrap test; Fig. 4e and Supplementary Fig. 14). When comparing non-target stimuli, the fractions of discriminative cells were similar across cell types, which is not the case in task-performing animals. These results demonstrate further that sensory stimulus features alone are not sufficient to explain the different activation patterns observed in S2P and M1P neurons under distinct task conditions.

In conclusion, we show that activity in S1 can be routed selectively to different cortical areas based on the sensory processing requirements for the execution of specific tasks. The prominent recruitment of S2P neurons during texture discrimination compared to that during object localization may reflect the activation of higher sensory areas[2] for processing more complex sensory stimuli[25,26]. In contrast, M1P neurons show an increased response to, and ability to discriminate, pole position during object localization. Although the behaviour strategy used by the animal ('active sensing' versus 'detection amid distractors')[22,24] cannot be distinguished, our activation patterns are in line with previous reports indicating that S1–M1 integration may inform the decision of the mouse under this task condition[18–20]. As sensory stimulus features alone are not sufficient to produce these differential activation patterns among S2P and M1P neurons, we speculate that other mechanisms could be involved, including plasticity of local and long-range circuits during task learning[27,28] or top-down influences exerted by feedback circuits or attention-related brain areas during task engagement[29,30]. Understanding the circuits and mechanisms underlying this selective routing of sensory information will warrant further investigation.

METHODS SUMMARY

Young adult male transgenic Cre-dependent tdTomato reporter mice (P35-42) were injected with virus expressing YC-Nano140 into S1 and retrograde virus expressing Cre into S2. A cranial window was implanted over S1, along with a head post for head fixation. After a recovery period of 1 week, animals were habituated to head fixation and trained in the texture-discrimination or object-localization task, respectively. In separate experiments, sandpaper or a pole were presented to naive animals under similar task conditions but with reward and punishment removed. The principal whisker corresponding to imaging areas in YC-Nano140 expression regions was identified by intrinsic signal optical imaging. *In vivo* two-photon calcium imaging (7 Hz) in S1, along with high-speed videography (500 Hz) of motion and touch of all contralateral whiskers was carried out on animals, 3 to 4 weeks post injection. Trained mice were imaged twice a day for up to 16 behaviour sessions. Untrained mice were imaged for one session each of sandpaper and pole presentation. Animals were injected with CTB-Alexa647 into M1 after the last imaging session, then perfused and fixed after 5 to 7 days with 4% paraformaldehyde. GABA immunohistochemistry was carried out on fixed tissue sections cut parallel to the imaging plane. *In vivo* imaged areas were located in post-hoc sections to identify M1P neurons and GABAergic interneurons. Data analysis

was performed with ImageJ and MATLAB. Behaviour and whisker kinematic vectors were obtained by analysis of high-speed videos of whisker movement. Cells were classified according to behaviour using cross-correlation analysis of calcium signals and behaviour vectors. Single-cell discrimination of decision or stimulus was performed using a ROC analysis.

Full Methods and any associated references are available in the online version of the paper.

Received 27 September 2012; accepted 30 April 2013.
Published online 23 June 2013.

1. Diamond, M. E., von Heimendahl, M., Knutsen, P. M., Kleinfeld, D. & Ahissar, E. 'Where' and 'what' in the whisker sensorimotor system. *Nature Rev. Neurosci.* **9,** 601–612 (2008).
2. Felleman, D. J. & Van Essen, D. C. Distributed hierarchical processing in the primate cerebral cortex. *Cereb. Cortex* **1,** 1–47 (1991).
3. Aronoff, R. *et al.* Long-range connectivity of mouse primary somatosensory barrel cortex. *Eur. J. Neurosci.* **31,** 2221–2233 (2010).
4. Mao, T. *et al.* Long-range neuronal circuits underlying the interaction between sensory and motor cortex. *Neuron* **72,** 111–123 (2011).
5. Sato, T. R. & Svoboda, K. The functional properties of barrel cortex neurons projecting to the primary motor cortex. *J. Neurosci.* **30,** 4256–4260 (2010).
6. Chakrabarti, S. & Alloway, K. D. Differential origin of projections from SI barrel cortex to the whisker representations in SII and MI. *J. Comp. Neurol.* **498,** 624–636 (2006).
7. Madisen, L. *et al.* A robust and high-throughput Cre reporting and characterization system for the whole mouse brain. *Nature Neurosci.* **13,** 133–140 (2010).
8. Horikawa, K. *et al.* Spontaneous network activity visualized by ultrasensitive Ca^{2+} indicators, yellow Cameleon-Nano. *Nature Methods* **7,** 729–732 (2010).
9. Carvell, G. E. & Simons, D. J. Biometric analyses of vibrissal tactile discrimination in the rat. *J. Neurosci.* **10,** 2638–2648 (1990).
10. Guic-Robles, E., Jenkins, W. M. & Bravo, H. Vibrissal roughness discrimination is barrel cortex-dependent. *Behav. Brain Res.* **48,** 145–152 (1992).
11. Jadhav, S. P., Wolfe, J. & Feldman, D. E. Sparse temporal coding of elementary tactile features during active whisker sensation. *Nature Neurosci.* **12,** 792–800 (2009).
12. von Heimendahl, M., Itskov, P. M., Arabzadeh, E. & Diamond, M. E. Neuronal activity in rat barrel cortex underlying texture discrimination. *PLoS Biol.* **5,** e305 (2007).
13. Crochet, S. & Petersen, C. C. Correlating whisker behavior with membrane potential in barrel cortex of awake mice. *Nature Neurosci.* **9,** 608–610 (2006).
14. Fee, M. S., Mitra, P. P. & Kleinfeld, D. Central versus peripheral determinants of patterned spike activity in rat vibrissa cortex during whisking. *J. Neurophysiol.* **78,** 1144–1149 (1997).
15. Curtis, J. C. & Kleinfeld, D. Phase-to-rate transformations encode touch in cortical neurons of a scanning sensorimotor system. *Nature Neurosci.* **12,** 492–501 (2009).
16. O'Connor, D. H., Peron, S. P., Huber, D. & Svoboda, K. Neural activity in barrel cortex underlying vibrissa-based object localization in mice. *Neuron* **67,** 1048–1061 (2010).
17. de Kock, C. P., Bruno, R. M., Spors, H. & Sakmann, B. Layer- and cell-type-specific suprathreshold stimulus representation in rat primary somatosensory cortex. *J. Physiol. (Lond.)* **581,** 139–154 (2007).
18. Petreanu, L. *et al.* Activity in motor-sensory projections reveals distributed coding in somatosensation. *Nature* **489,** 299–303 (2012).
19. Xu, N. L. *et al.* Nonlinear dendritic integration of sensory and motor input during an active sensing task. *Nature* **492,** 247–251 (2012).
20. Hill, D. N., Curtis, J. C., Moore, J. D. & Kleinfeld, D. Primary motor cortex reports efferent control of vibrissa motion on multiple timescales. *Neuron* **72,** 344–356 (2011).
21. Green, D. M. & Swets, J. A. *Signal Detection Theory and Psychophysics* (Wiley, 1966).
22. O'Connor, D. H. *et al.* Vibrissa-based object localization in head-fixed mice. *J. Neurosci.* **30,** 1947–1967 (2010).
23. Huber, D. *et al.* Multiple dynamic representations in the motor cortex during sensorimotor learning. *Nature* **484,** 473–478 (2012).
24. Mehta, S. B., Whitmer, D., Figueroa, R., Williams, B. A. & Kleinfeld, D. Active spatial perception in the vibrissa scanning sensorimotor system. *PLoS Biol.* **5,** e15 (2007).
25. Melzer, P., Champney, G. C., Maguire, M. J. & Ebner, F. F. Rate code and temporal code for frequency of whisker stimulation in rat primary and secondary somatic sensory cortex. *Exp. Brain Res.* **172,** 370–386 (2006).
26. Alloway, K. D. Information processing streams in rodent barrel cortex: the differential functions of barrel and septal circuits. *Cereb. Cortex* **18,** 979–989 (2008).
27. Guic, E., Carrasco, X., Rodriguez, E., Robles, I. & Merzenich, M. M. Plasticity in primary somatosensory cortex resulting from environmentally enriched stimulation and sensory discrimination training. *Biol. Res.* **41,** 425–437 (2008).
28. Wiest, M. C., Thomson, E., Pantoja, J. & Nicolelis, M. A. Changes in S1 neural responses during tactile discrimination learning. *J. Neurophysiol.* **104,** 300–312 (2010).
29. Krupa, D. J., Wiest, M. C., Shuler, M. G., Laubach, M. & Nicolelis, M. A. Layer-specific somatosensory cortical activation during active tactile discrimination. *Science* **304,** 1989–1992 (2004).
30. Gilbert, C. D. & Sigman, M. Brain states: top-down influences in sensory processing. *Neuron* **54,** 677–696 (2007).

Supplementary Information is available in the online version of the paper.

Acknowledgements We thank S. Soldado-Magraner and L. Sumanovski for assistance with data analysis, H. Kasper, M. Wieckhorst, S. Giger and F. Voigt for technical assistance, A. Miyawaki for plasmid reagents, and D. Margolis, H. Lütcke and K. Schulz for help with initial experiments, helpful discussions and comments on the manuscript and V. Padrun and F. Pidoux for virus production. This work was supported by grants from the Swiss National Science Foundation (310030-127091 to F.H.), the EU-FP7 program (PLASTICISE project 223524 to F.H. and B.L.S.; and the BRAIN-I-NETS project 243914 to F.H.), the Swiss SystemsX.ch initiative (project 2008/2011-Neurochoice to F.H. and B.L.S.), the National Center of Competence in Research 'Neural Plasticity and Repair' (F.H.), Forschungskredit of the University of Zurich (grant 541541808 to J.L.C.) and a fellowship from the US National Science Foundation, International Research Fellowship Program (grant 1158914 to J.L.C.).

Author Contributions J.L.C. and F.H. designed the study. J.L.C. carried out experiments. J.L.C., S.C., J.S.M and F.H. performed data analysis. S.C. carried out experiments and data analysis characterizing YC-Nano140. B.L.S. contributed viral reagents. J.L.C. and F.H. wrote the paper.

Author Information Reprints and permissions information is available at www.nature.com/reprints. The authors declare no competing financial interests. Readers are welcome to comment on the online version of the paper. Correspondence and requests for materials should be addressed to F.H. (helmchen@hifo.uzh.ch).

METHODS

Generation of viral construct. For the construction of the *pAAV-EF1α-YC-Nano140* viral construct, a *YC-Nano140* insert with 5′ BamHI and 3′ EcoRI restriction sites was generated by polymerase chain reaction (PCR) amplification from a *pcDNA3-YC-Nano140* vector[8] and subcloned into an *pAAV-EF1α-dio-eYFP* plasmid[31]. The *pAAV-pgk-Cre* construct has been described previously[3]. Recombinant serotype 6 AAV particles were produced by co-transfecting AAV-293 cells with the shuttle plasmid and the *pDP6* packaging plasmid. Cell lysates were subjected to purification on iodixanol density gradients followed by HPLC with HiTrap Heparin column (GE Healthcare Bio-Sciences AB) using standard procedures. The viral suspension that was obtained was concentrated using Centricon centrifugal filter devices with a molecular weight cut-off of 100 kilodaltons (kDa) (Millipore), and the suspension medium was replaced with PBS. Vector titres were determined by measuring the number of encapsidated genomes per ml using real-time PCR.

Viral and tracer injections. Experimental procedures were carried out following the guidelines of the Veterinary Office of Switzerland and were approved by the Cantonal Veterinary Office in Zurich. Stereotaxic viral and tracer injections were performed on young adult (postnatal day 35 to 42) male transgenic Cre-dependent tdTomato reporter mice (*ROSA26tm14(CAG-tdTomato)*, Ai14) as described previously[32]. AAV6-*EF1α-YC-Nano140* (300 nl, approximately 1×10^9 vg μl^{-1}) was delivered into S1, targeting L2/3 (1.1 mm posterior to bregma, 3.3 mm lateral, approximately 300 μm below the pial surface). AAV6-*pgk-Cre* (300 nl, approximately 1×10^9 vg μl^{-1}) was delivered into S2, targeting L2/3 and L5 (0.7 mm posterior to bregma, 4.2 mm lateral, approximately 300 and 500 μm below the pial surface). CTB-Alexa647 (Molecular Probes, Invitrogen; 300 nl, 1% wt/vol) was injected into M1 immediately after the last behaviour imaging session, targeting L2/3 and L5 (1.2 mm anterior to bregma, 0.6 mm lateral, approximately 300 and 500 μm below the pial surface).

Cranial window implantation and habituation. To allow long-term *in vivo* calcium imaging, a cranial window was implanted 24 h after virus injections over S1 as described[33]. A metal post for head fixation was implanted on the skull, contralateral to the cranial window, using dental acrylic. One week after chronic window implantation, mice were handled daily for 1 week while they became acclimatized to a minimum of 15 min of head fixation. Mice were water restricted for the remainder of the experiment.

Texture-discrimination and object-localization tasks. Behaviour experiments were performed using a data acquisition interface (USB-6008; National Instruments) and custom-written LabVIEW software (National Instruments) to control devices required for the task and for recording trial and licking data. Licking of a water port mounted to a piezo film sensor (MSP1006-ND; Measurement Specialties) triggered delivery of water (5 to 6 μl) through a miniature rocker solenoid valve (0127; Buerkert). Mice were initially trained during two sessions to trigger water reliably by licking the lick port, and then progressed to go/no-go task training. For texture discrimination, commercial-grade sandpaper (3M) was used. Rough sandpaper (P100) served as a target stimulus and sandpapers of increasing smoothness (P280, P600, P1200) served as non-target stimuli. Sandpapers were mounted onto panels attached to a stepper motor (T-NM17A04; Zaber) mounted onto a motorized linear stage (T-LSM100A; Zaber) to move textures in and out of reach of whiskers. For object localization, a 1.6-mm diameter pole was mounted onto a pneumatic linear slider (SLS-10-30-P-A Mini slide; Festo) to bring the pole in and out of reach of the whiskers rapidly[22]. This device was mounted on the same motorized linear stage used for texture discrimination to position the pole at target and non-target locations (4.29 mm or 6 mm anterior to the target location), all within reach of the whiskers. Go and no-go trials were presented randomly with a 50% probability of each trial type, and with a maximum of three consecutive presentations of the same trial type. A trial consisted of a 3-s pre-stimulus period followed by stimulus presentation for a maximum of 2 s accompanied by an intermittent 2,093-Hz auditory cue tone. Licking during target stimulus presentation was scored as a 'hit' and triggered immediate withdrawal of the stimulus accompanied by water delivery paired with a 2,093- and 2,793-Hz auditory reward tone. When there was no lick, this was scored as a 'miss', and the next trial followed immediately. During presentation of non-target stimuli, a no-lick response was scored as a 'correct rejection', and the next trial followed immediately; and licking was scored as a 'false alarm', in which case the stimulus was withdrawn immediately, no water reward was given, and the animal was punished with a light air puff to the face and a 7-s time-out period accompanied by auditory white noise. A sensitivity index of animal performance (d') was calculated for all trials per session as $d' = Z(\text{Hit}/(\text{Hit} + \text{Miss})) - Z(\text{FA}/(\text{FA} + \text{CR}))$, where Hit and Miss are the numbers of hits and misses, respectively, CR is the number of correct rejections, FA is the number of false alarms. $Z(p)$, $p \in [0,1]$ is the inverse of the cumulative Gaussian distribution, where p is Hit/(Hit + Miss) or FA/(FA + CR). Imaging during behaviour began once animals reached a performance level of $d' > 1.75$ (80% correct) for one session. All training and imaging sessions occurred twice per day. For passive presentation of sandpaper or pole in untrained animals, a similar trial structure was used as during task conditions, with the lick port removed and no reward or punishment given. For both trained and untrained animals, stimuli were presented at positions in which whisker contact could occur under both non-whisking and whisking conditions.

Intrinsic signal optical imaging. The S1 barrel column corresponding to the YC-Nano140 expression area was identified using intrinsic signal optical imaging under approximately 1.5% isoflurane anaesthesia. The cortical surface was illuminated with a 630-nm light-emitting diode (LED), single whiskers were stimulated (2 to 4° rostrocaudal deflections at 10 Hz), and reflectance images were collected through a ×4 objective with a CCD camera (Toshiba TELI CS3960DCL; 12-bit; 3-pixel binning, 427 × 347 binned pixels, 8.6-μm pixel size, 10-Hz frame rate). Intrinsic signal changes were computed as fractional changes in reflectance relative to the pre-stimulus average (50 frames; expressed as $\Delta R/R$). The centres of the barrel columns corresponding to stimulated whiskers were located by averaging intrinsic signals (15 trials), median-filtering (5-pixel radius) and thresholding to find signal minima. Reference surface vasculature images were obtained using 546-nm LED and matched to images acquired during two-photon imaging. All whiskers, with the exception of principal and first-order surround whiskers corresponding to the expression area, were partially trimmed prior to behaviour training, to a length at which they were out of reach from pole or texture contact during the task. During whisker trimming, the principal whisker was noted by images taken from the high-speed video camera for re-identification in subsequent imaging sessions for whisker tracking.

Two-photon imaging. We used a custom-built two-photon microscope controlled by HelioScan[34], equipped with a Ti:sapphire laser system (approximately 100-femtosecond (fs) laser pulses; Mai Tai HP; Newport Spectra Physics), a water-immersion objective (×40 LUMPlanFl/IR, 0.8 NA; Olympus), galvanometric scan mirrors (model 6210; Cambridge Technology), and a Pockel's Cell (Conoptics) for laser intensity modulation. For initial identification of YC-Nano140-expressing and tdTomato-positive S2P neurons, a volume stack was acquired using 800-nm excitation and yellow (542/50 nm) and red (610/75 nm) emission filters, respectively (AHF Analysentechnik). For calcium imaging, YC-Nano140 was excited at 840 nm and fluorescence was collected with blue (480/60 nm) and yellow (542/50 nm) emission filters. Images were acquired at 7 Hz with 180 × 180 or 256 × 128 pixel resolution. Single trials of 6 to 7 s duration were recorded, with 1-s breaks between trials to allow for hard-disk storage during inter-trial periods.

Whisker tracking. The whisker field was illuminated with a 940-nm infrared LED light and videos were acquired at 500 Hz (500 × 500 pixels) using a high-speed CMOS camera (A504k; Basler). The average whisker angle across all imaged whiskers was measured using automated whisker-tracking software[35]. For all trials, the duration of whisker to texture or pole contact was quantified manually through visual inspection. For a random subset of trials (approximately 80% of correct-rejection trials for texture discrimination, approximately 66% of hit and correct-rejection trials for object localization), the position of the principal whisker tip was tracked manually over a 1,100-ms time period starting 100 ms before the initial touch.

Post-hoc immunohistochemistry. After a period of five to seven days after CTB-Alexa647 injection (to allow uptake)[36], mice were anaesthetized (ketamine and xylazine; 100 mg per kg and 20 mg per kg body weight) and perfused transcardially with 4% paraformaldehyde in phosphate buffer, pH 7.4. Cortical sections (50 μm) were cut along the imaging plane using a vibratome (VT100; Leica), then blocked in 10% normal goat serum (NGS) and 1% Triton at room temperature and incubated overnight at 4 °C in 5% NGS, 0.1% Triton, and the following primary antibodies: green fluorescent protein (GFP) (rat monoclonal antibody; 1:5,000; Nacalai) and GABA (rabbit polyclonal antibody; 1:1,000; Sigma). Appropriate Alexa488- and Alexa405-conjugated goat immunoglobulin-G (IgG) secondary antibodies (1:400; Molecular Probes, Invitrogen) were applied for 2 h at room temperature (approximately 22 °C). Images were acquired with a confocal microscope (Fluoview 1000; Olympus) with respective ultraviolet (GABA), green (YC-Nano140), red (tdTomato) and infrared (CTB-Alexa647) excitation or emission filters.

Calcium-imaging analysis. Two-channel (cyan fluorescent protein (CFP) and yellow fluorescent protein (YFP)) calcium-imaging data were imported into MATLAB (Mathworks) for processing. First, the background was subtracted on each channel (bottom 1st percentile fluorescence signal across the entire frame). Hidden Markov model line-by-line motion correction was applied to both data channels[37]. Regions of interest (ROIs) corresponding to individual neurons were selected manually from the mean image of a single-trial time series using ImageJ (National Institutes of Health). Mean pixel value for each ROI was extracted for both channels. Calcium signals were expressed as relative YFP:CFP ratio change $\Delta R/R = (R - R_0)/R_0$. R_0 was calculated for each trial as the bottom 8th percentile of

the ratio for the trial. Active neurons were identified by two-way ANOVA with repeated measures of the neuronal calcium signal against the neuropil signal (significance value, $P < 0.05$). Owing to a number of factors—including variations in awake imaging conditions, variable noise levels across neuronal populations in the field of view, and slow decay kinetics of YC-Nano140 (Supplementary Fig. 3)—detection of calcium transients reflecting single action potentials is unlikely to occur with 100% fidelity during experimental conditions. Using a deconvolution approach, we obtained estimates of the action-potential firing-rate changes underlying the observed calcium signals as well as of the total number of extra action potentials evoked during the trial period (Supplementary Figs 3 and 8, and Supplementary Methods).

Behaviour classification. Behaviour vectors were constructed as follows. Owing to the relatively slow kinetic properties of YC-Nano140 and the low image acquisition rate (7 Hz) compared to observed whisking frequency (8 to 12 Hz)[13,14,20,38], measured calcium signals are unlikely to reflect whisking frequency accurately or to distinguish slow changes in whisking amplitude from fast rhythmic variation in position[15,20]. As rhythmic and non-rhythmic whisking occurred (Supplementary Video 3), whisking amplitude was used as a measure to represent both forms of whisking behaviour. The envelope of whisking amplitude was calculated as the difference between maximum and minimum whisker angles along a sliding window equal to the imaging frame duration (142 ms). For whisker touch, a binary vector was constructed to represent whisker contact periods. Both vectors were downsampled to the 7-Hz imaging rate. Using MATLAB, cross correlation of behaviour vectors and cellular calcium signal vectors was performed across the entire behaviour session, with all trials concatenated into single vectors with n elements. For two time-series vectors, $\boldsymbol{x}$ and $\boldsymbol{y}$, covariance across lags $k = 0, \pm1, \pm2$ frames was calculated as:

$$c_{xy}\begin{cases}\frac{1}{n}\sum_{t=1}^{n-k}(x_t-\bar{x})(y_{t+k}-\bar{y}) & k=0,\ 1,\ 2\ldots\\ \frac{1}{n}\sum_{t=1}^{n+k}(y_t-\bar{y})(x_{t-k}-\bar{x}) & k=-1,\ -2\ldots\end{cases}$$

where $\bar{x}$ and $\bar{y}$ denote the means of $\boldsymbol{x}$ and $\boldsymbol{y}$ across all values. The sample cross-correlation (R value) was then computed as:

$$R_{xy}(k)=\frac{c_{xy}(k)}{\sigma_x\sigma_y} \qquad k=0,\ \pm1,\ \pm2\ldots$$

where σ_x and σ_y denote standard deviations of $\boldsymbol{x}$ and $\boldsymbol{y}$, respectively. To determine whether calcium signals of a neuron were significantly correlated to a given behaviour above chance levels, we carried out a random permutation test by shuffling individual time points along the calcium signal vector across the entire behaviour session. The sample cross correlation was then computed on this shuffled data set, and shuffling was repeated 1,000 times to obtain a distribution of R values from which confidence intervals and P values could be determined for significance tests.

To distinguish putative 'touch' and 'whisking' cells, we compared the R values from touch and whisking vectors statistically by bootstrapping with sample replacement. Calcium transients from individual trials were replaced randomly with transients of other trials from the same behaviour session. The sample cross correlation was then computed against the touch and whisking vector on this bootstrapped data set. This process was repeated 1,000 times to obtain 95% confidence intervals for significance tests. In general, correlations with positive time lags indicate that calcium signals follow behaviour, whereas correlations with negative time lags indicate that calcium signals precede behaviour (specifically, whisking cells are typically active before touch; Supplementary Fig. 8). The peak R value over the range of time lags analysed typically correlates to the peak of the calcium transient, as opposed to the calcium signal onset. Touch cells were identified as having a peak positive R value for touch above chance (from random permutation test) between lags $k = 0$ to 4 frames ($t = 0$ to 571 ms). This R value had to be significantly higher than the R value for whisking (from bootstrap test) at the corresponding time lag. As whisking signals show a delayed time to peak correlation, compared to touch signals[18], whisking cells were identified as having a peak positive R value for whisking between lags $k = 2$ to 5 frames ($t = 285$ to 714 ms). This R value had to be significantly higher than the R value for touch at the corresponding time lag. Cells with no significant correlation for touch or whisking were unclassified. Cells with a peak negative R value between lags $k = 0$ to 5 frames or a peak positive R value at $k > 5$ frames or $k < 0$ frames for both touch and whisking were also unclassified.

To determine the likelihood that the measured distribution of behaviour-classified neurons across S2P, M1P and unlabelled subtypes was above chance, a random permutation test was performed by shuffling the classification labels. For each permutation, the fraction of cells belonging to a particular behaviour classification was calculated. This process was repeated 1,000 times to obtain a distribution for each behaviour-subtype combination representing the null hypothesis that no behaviour-subtype dependencies exist. To compare the measured distribution of classified cells across S2P, M1P and unlabelled subtypes, bootstrapping with sample replacement of cells with a defined behaviour-subtype combination was performed 1,000 times to obtain 95% confidence intervals for each observed combination. The bias index for individual neurons in naive animals was calculated as $(R_{\text{sandpaper}} - R_{\text{pole}})/(R_{\text{sandpaper}} + R_{\text{pole}})$, where the R value represents the peak correlation within lags $k = 0$ to 4 frames ($t = 0$ to 571 ms) of the calcium signal to touch vector.

Whisker kinematic analysis. For analysis of kinematic parameters, 'slip' events were identified as described previously[11]. Principal whisker velocity and acceleration were determined by calculating the first and second derivative, respectively, of the time vector representing whisker-tip displacement. Slips were defined as events with both high positive acceleration and high absolute velocity, exceeding thresholds corresponding to four standard deviations above the means across all measured trials ($\Theta_A = 20.9\ \text{mm ms}^{-2}$ and $\Theta_V = 35.6\ \text{mm ms}^{-1}$). For texture discrimination, slips represent motion occurring as a result of the contact between whisker tip and texture surface as described previously[11]. During object localization, pole contact typically occurs along the whisker shaft. In this case, a high-acceleration, high-velocity event satisfying the criteria of a slip event occurs either following initial pole contact, producing a fast recoiling motion, or during full whisking behaviour when the whisker initially catches but bends past the pole, springing free. Whisker curvature change ($|\Delta\kappa|$), reflecting contact forces upon touch[39], was measured as the whisker curvature at each time point of touch minus the mean curvature over the 100-ms period before initial touch. Whisker curvature was determined as $\kappa = 1/R$, where R is the radius of a circle, in which the whisker length represents the arc length between the follicle and tip position and in which the direct distance between the follicle and tip position represents the chord. Whisker angle was calculated as the arctangent of $(x_{\text{follicle}} - x_{\text{tip}})/(y_{\text{follicle}} - y_{\text{tip}})$, where 0 degrees is orthogonal to the anterior–posterior axis.

For cross-correlation analysis of kinematic parameters to calcium signals, time vectors of kinematic parameters were downsampled to the imaging frame rate and analysis was carried out on the first second after initial touch (7 frames per trial) for correct-rejection trials. For slips, cross correlation was performed on a time vector corresponding to the cumulative number of slips over the time period. For curvature change, cross correlation was performed on a time vector representing the max $|\Delta\kappa|$ at each frame interval. For whisker angle, the time vector representing whisker angle was separated into eight binary vectors representing a range of angles from -90° to 90°, subdivided at 22.5° intervals. Each sub-vector reflects the likelihood that the whisker angle falls within that given angle range. Cross correlation was performed on each sub-vector and the overall correlation to whisker angle was obtained by taking the maximum R value across the eight sub-vectors. Owing to limited imaging speed, slow calcium-indicator kinetics, and because L2/3 neuronal activity in S1 is largely devoid of fast touch signals[15,16], measured calcium responses are not likely to represent instantaneous kinematic features. The correlation values obtained represent relative measures of response preferences to these parameters solely to permit a comparison across cell types.

Single-neuron discrimination analysis. The performance of single neurons in discriminating behavioural decisions or presented stimuli was assessed using a receiver operating characteristic (ROC) analysis[16,21]. Classification of decision X (or stimulus X) versus decision Y (stimulus Y) was based on the similarity of the calcium transient in each trial to the mean calcium transient for trial type X compared to trial type Y. Only the first second of the calcium signals following initial texture or pole contact was considered. Each trial was assigned a 'discrimination variable' score (DV) equal to the dot-product similarity to the mean calcium transient for trial type X minus the dot-product similarity to the mean for trial type Y. Thus, for trial type X:

$$\text{DV}_X = X_i\left(\bar{X}_{\forall j\neq i} - \bar{Y}\right)$$

and for trial type Y:

$$\text{DV}_Y = Y_i\left(\bar{X} - \bar{Y}_{\forall j\neq i}\right)$$

where X_i and Y_i are the single-trial calcium transients for the i-th trial. $\bar{X}$ and $\bar{Y}$ are the mean 1-s calcium transients after initial texture or pole contact for the respective trial type (with the trial under consideration omitted for averaging). Trials were classified as belonging to trial type X or Y if DV_X or DV_Y was greater than a given criterion, respectively. To determine the fraction of trials an ideal observer could correctly classify, a ROC curve was constructed by varying this criterion value across the entire range of DV_X or DV_Y. At each criterion value, the probability that a trial of type X exceeded the criterion value was plotted against the probability that a trial of type Y exceeded the criterion value. The area under the ROC curve was then calculated to represent the single-neuron performance ('fraction correct') as the fraction of trials correctly discriminated by an ideal observer using the DV[21].

Neurons that discriminated above chance were identified using repeated permutations tests in which decision or stimulus labels were randomly shuffled. For each permutation test, a threshold corresponding to the shuffled distribution 0.95 percentile was calculated. Neurons, whose performance values were above the mean value of this threshold across 1000 permutation tests, were considered to be discriminating above chance.

31. Gradinaru, V. *et al.* Molecular and cellular approaches for diversifying and extending optogenetics. *Cell* **141,** 154–165 (2010).
32. Lütcke, H. *et al.* Optical recording of neuronal activity with a genetically-encoded calcium indicator in anesthetized and freely moving mice. *Front Neural Circuits* **4,** 9 (2010).
33. Margolis, D. J. *et al.* Reorganization of cortical population activity imaged throughout long-term sensory deprivation. *Nature Neurosci.* **15,** 1539–1546 (2012).
34. Langer, D. *et al.* HelioScan: A software framework for controlling in vivo microscopy setups with high hardware flexibility, functional diversity and extendibility. *J. Neurosci. Methods* **215,** 38–52 (2013).
35. Knutsen, P. M., Derdikman, D. & Ahissar, E. Tracking whisker and head movements in unrestrained behaving rodents. *J. Neurophysiol.* **93,** 2294–2301 (2004).
36. Conte, W. L., Kamishina, H. & Reep, R. L. Multiple neuroanatomical tract-tracing using fluorescent Alexa Fluor conjugates of cholera toxin subunit B in rats. *Nature Protocols* **4,** 1157–1166 (2009).
37. Dombeck, D. A., Khabbaz, A. N., Collman, F., Adelman, T. L. & Tank, D. W. Imaging large-scale neural activity with cellular resolution in awake, mobile mice. *Neuron* **56,** 43–57 (2007).
38. de Kock, C. P. & Sakmann, B. Spiking in primary somatosensory cortex during natural whisking in awake head-restrained rats is cell-type specific. *Proc. Natl Acad. Sci. USA* **106,** 16446–16450 (2009).
39. Birdwell, J. A. *et al.* Biomechanical models for radial distance determination by the rat vibrissal system. *J. Neurophysiol.* **98,** 2439–2455 (2007).